TÜBİTAK

Turkish Journal of Earth Sciences

http://journals.tubitak.gov.tr/earth/

Research Article

Turkish J Earth Sci
(2018) 27: 110-126

doi:10.3906/yer-1707-16

Morphotectonic analysis of the East Anatolian Fault, Turkey

Abdelrahman KHALIFA[1,2,*], Ziyadin ÇAKIR[1], Lewis A. OWEN[2], Şinasi KAYA[3]

[1]Department of Geological Engineering, Faculty of Mines, İstanbul Technical University, İstanbul, Turkey
[2]Department of Geology, University of Cincinnati, Cincinnati, Ohio, USA
[3]Department of Geomatics, Faculty of Civil Engineering, İstanbul Technical University, İstanbul, Turkey

Received: 21.07.2017 • **Accepted/Published Online:** 29.01.2018 • **Final Version:** 19.03.2018

Abstract: The East Anatolian Fault (EAF) is a morphologically distinct and seismically active left-lateral strike-slip fault that extends for ~400 km and forms the Arabian/Anatolian plate boundary in southeastern Turkey. The EAF together with its conjugate fault, the North Anatolian Fault, help accommodate the westward escape of the Anatolian plate from the Arabian/Eurasian collision zone. Morphotectonic features along the EAF provide insights into the nature of landscape development and aid in understanding variations in tectonic activity and fault evolution. Several geomorphic indices, namely stream length-gradient index, mountain-front sinuosity, valley width to valley height ratio, basin asymmetry factor, and drainage density, and hypsometric analysis were examined using digital elevation models**.** The EAF can be divided into five segments based on its tectonic geomorphology. The stream length-gradient index values are between 50 and 350 along the five segments. Mountain-front sinuosity varies from 1.01 to 1.46 on the five segments. The mean ratio of valley floor width to valley height along the studied segments ranges from 0.11 to 1.32, which is well correlated with the mountain-front sinuosity values. Basin asymmetry factors for 18 catchments range from 1.88 to 26.25 along the study fault zone. Drainage density values for the studied catchments range from 3.5 to 5.6. Finally, the hypsometric analysis index of the 18 catchments indicates high, intermediate, and low relative tectonic activity. The results show that all geomorphic indices are remarkably uniform along the entire length of the fault, thus indicating that fault development was essentially coeval along its length, which supports the view that the present-day Arabian/Anatolian plate boundary (delimited by the EAF) jumped eastwards from the Malatya-Ovacık Fault at ~3 Ma. This is in good agreement with the nearly uniform geological offsets and the GPS-determined present-day slip rate of ~10 mm/year along the entire fault.

Key words: Geomorphic indices, morphometric analysis, tectonic geomorphology, East Anatolian Fault

1. Introduction

Analysis of drainage systems and landforms along active faults provides important insights into fault evolution and present-day tectonic activity. Numerous field and laboratory studies have been conducted to examine how drainage systems evolve along strike-slip faults, uplifting blocks, and evolving thrusts and folds (Azor et al., 2002; El Hamdouni et al., 2008; Castelltort et al., 2012; Özkaymak and Sözbilir, 2012; Ul-Hadi et al., 2013; Yıldırım, 2014; Tari and Tüysüz, 2015; Topal et al., 2016; Khalifa et al., 2017; Tepe and Sözbilir, 2017). The distinction between active and inactive faults can be inferred through detailed studies of geomorphic indices, including stream length-gradient index (S_L), mountain-front sinuosity (S_{mf}), valley floor width to height ratios (V_f), drainage density (D_d), and hypsometric integral (H_i) (Owen et al., 1999; Keller and DeVecchio, 2013). Studies on tectonic geomorphology, mountain uplift, and drainage development along continental-scale strike-slip faults are scarce (e.g., Michael and Frank, 2013).

The East Anatolian Fault (EAF), a morphologically distinct and seismically active left-lateral strike-slip fault that extends for ~400 km, forming a plate boundary between the Arabian and Anatolian plates in southeastern Turkey, provides an excellent natural laboratory for the study of continental-scale strike-slip fault systems (Figure 1). We examined the tectonic geomorphology along the entire EAF using a number of geomorphic indices to gain insights into the recent evolution of this plate boundary and to expand our understanding of the tectonic geomorphology of continental-scale strike-slip faults. We determine, e.g., if there is a direction in fault propagation similar to the North Anatolian Fault (NAF) (which is from east to west according to Şengör et al., 2014), reveal along-strike variation in the fault activity, and discuss the implications for tectonic evolution of the region.

* Correspondence: akhalifa@itu.edu.tr

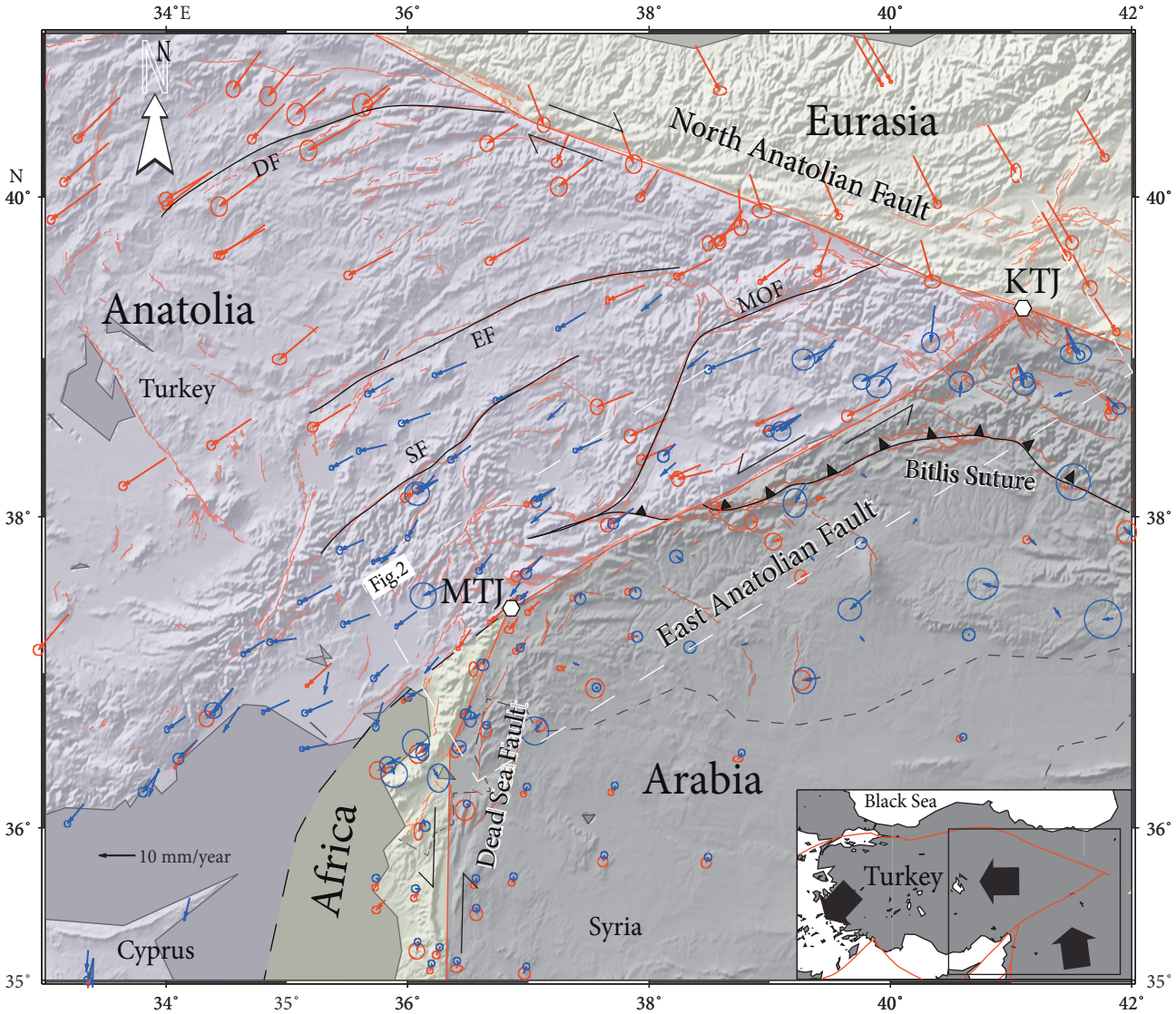

Figure 1. Shaded relief image (data from SRTM-30; Farr et al., 2007) of eastern Turkey showing the African, Arabian, Anatolian, and Eurasian plates and major active faults (thick black and red lines). Red and blue arrows indicate GPS velocities with respect to a fixed Arabian plate, with blue and red circles indicating GPS measurements errors, according to Reilinger et al. (2006) and Aktuğ et al. (2016), respectively. MTJ, Maraş triple junction; KTJ, Karlıova triple junction; DF, Deliler fault; EF, Ecemiş fault; SF, Savrun fault; MOF, Malatya-Ovacık fault. The inset map and box with white dashed lines show location of the study area and Figure 2, respectively.

2. Seismotectonic setting

The left-lateral strike-slip EAF extends between the Karlıova and Maraş triple junctions and connects the NAF and the Dead Sea Fault in southeastern Turkey to form the boundary between the Anatolian and Arabian lithospheric plates (Şengör, 1979; Reilinger et al., 2006), (Figure 1). Together with the right-lateral conjugate NAF, the EAF accommodates the westward escape of the Anatolian plate from the collisional Arabian/Eurasian plate boundary (McKenzie, 1972; Şengör, 1979). The EAF transform behavior was first recognized and described by Allen (1969), and it was mapped by Arpat and Şaroğlu (1972). The EAF dominated the regional tectonics and seismicity during the Quaternary in central Turkey and has been examined by many researchers (Arpat and Şaroğlu, 1975; McKenzie, 1976, 1978; Jackson and McKenzie, 1984; Dewey et al., 1986; Muehlberger and Gordon, 1987; Westaway, 1994; Westaway and Arger, 1996; Reilinger et al., 2006; Duman and Emre, 2013; Aktuğ et al., 2016; Yönlü et al., 2017). Fault-controlled catchments along the EAF contain Pliocene lignite. The age of the lignite brackets the onset of fault activity to between the late Miocene and earliest Pliocene (Arpat and Şaroğlu, 1972; Hempton, 1985; Şengör et al., 1985; Dewey et al., 1986).

The estimates of the accumulated overall offset along the EAF vary between an upper range of 27–33 km that is recorded by geological features and the length of the Gölbaşı strike-slip basin (Westaway and Arger, 1996; Bulut et al., 2012) and a lower range of 15–22 km that is defined by drainage channel offsets on individual fault segments (Hempton, 1987; Bulut et al., 2012). Studies based on the geologic and geomorphic data along the EAF provide slip rates of between 6 and 11 mm/year (Arpat and Şaroğlu, 1975; Kiratzi, 1993; Westaway, 1994; Yürür and Chorowicz, 1998; Çetin et al., 2003; Aksoy et al., 2007; Herece, 2008; Duman and Emre, 2013, Yönlü et al., 2013), whereas GPS studies provide a constant slip rate of ~10 mm/year along the whole EAF (Reilinger et al., 2006; Mahmoud et al., 2013; Aktuğ et al., 2016).

The Malatya and Ovacık faults located to the north of the EAF are secondary structures with left-lateral sense of slip within the study region. Koçyiğit and Beyhan (1998) and Kaymakcı et al. (2006) considered the different segments of the Malatya and Ovacık fault to be part of the Malatya-Ovacık Fault Zone (MOFZ) (Figure 1), whose present-day activity is debated by Jackson and McKenzie (1984), Westaway and Arger (1996, 2001), Koçyiğit and Beyhan (1998), and Kaymakcı et al. (2006). Westaway and Arger (2001) interpreted the SW- and SSW-trending segments of the MOFZ as transform faults and argued for ~240 km left-lateral along the MOFZ, making it one of the major fault zones in eastern Turkey. Based on the geometry of the former Erzincan triple junction, which differs from the modern Karlıova triple junction, Westaway and Arger (2001) suggested that the MOFZ is no longer active. Some researchers, e.g., Jackson and McKenzie (1984) and Westaway and Arger (1996, 2001), stated that the EAF was initiated and at the same time the significant movement of the MOFZ ceased at the end of the Early Pliocene (~3 Ma). In contrast, Koçyiğit and Beyhan (1998) and Kaymakcı et al. (2006) claimed that the MOFZ is still active.

The evolution of the Euphrates River, offset by the EAF, can be summarized as follows. After activity along the MOFZ ceased, lacustrine sedimentation smoothed out the surface relief, leaving a subdued topographic low along the line of the MOFZ. Then drainage started to develop along the length of the MOFZ to form the modern Euphrates gorge that crosses the EAF, which now provides the outlet from the Malatya basin (Westaway and Arger, 2001). The Euphrates River was then offset ~13 km by the EAF. However, the total slip on this strand is debated, with estimates up to ~30 km (Westaway, 1994; Westaway and Arger, 2001). Westaway and Arger (2001) argued that the modern Euphrates River began to form at ~1.3–3 Ma, with the assumption that the majority of the gorge development occurred in the last 1 Ma. Thus, a long-term slip-rate for the EAF of ~8.3 mm/year is based on the offset of the Euphrates River for the past 3 Ma (Herece and Akay, 1992).

Movement of the EAF produces large earthquakes, which seem to occur along the fault every few hundred years in various places, within relatively short paroxysmal periods of large events (Ambraseys, 1988). Recently, the most significant and destructive earthquake occurred on 22 May 1971 near Bingöl with M_w of 6.6 and focal depth of ~10 km (Taymaz et al., 1991).

Recent seismicity was studied by Bulut et al. (2012), who identified normal and thrust faulting events in all segments of the EAF and stated that the orientations of the nodal planes of the focal mechanisms of these events indicate off-fault subsidiary fault segments that fit to the overall EAF kinematics. Bulut et al. (2012) suggested that the mechanisms of the EAF are compatible with thrust and normal faulting events, depending on the trend of the respective earthquakes hypocenters.

3. Segmentation of the East Anatolian Fault

Segmentation of the EAF has been examined by many researchers. Hempton et al. (1981), e.g., classified the EAF into 5 segments according to the variations in trend and geometry of the fault. Barka and Kadinsky-Code (1988) suggested 14 segments between Karlıova and Türkoğlu based on geometric discontinuities, surface ruptures, and seismicity. Şaroğlu et al. (1992a) recorded six segments based on changes in strike of the fault trace. Duman and Emre (2013) divided the main strand of the EAF into 13 segments based on fault jogs and abrupt changes in the strike of the fault trace. According to Duman and Emre (2013), the EAF can be divided into five segments between Karlıova and Türkoğlu, which from east to west are named Karlıova (Karlıova–Bingöl), Palu (Palu–Sivrice), Pütürge (Sivrice–Çelikhan), Erkenek (Çelikhan–Gölbaşı), and Pazarcık (Gölbaşı–Türkoğlu), which we call segments 1 through 5 (Figure 2).

Left-lateral faulted landforms, such as displaced streams, are common along segment 1 (Karlıova). In two areas, north of Sakaören and south of Serpmekaya (Figure 3a), the fault traverses alluvial plains and fans, and fresh fault scarps are evident along its length (Duman and Emre, 2013). In this segment, streams are left-laterally offset by several to a few hundred meters (Herece, 2008). This includes a 3.5-m-horizontal left-lateral offset of the fault trace recorded by Ambraseys and Jackson (1998) some 1 km southeast of Boncukgöze (Figure 3a). This is probably a surface rupture of the M_w 7.1 1866 earthquake. The Karlıova segment contains the Gökdere bend, which is a large right step within the EAF zone that has produced a push-up hill. The eastern and western parts of the step have NE-SW and E-W trending folds, thrusts, and strike-slip faults (Duman and Emre, 2013). A series of thrust faults occur in the southern part of the push-up structure (Duman and Emre, 2013).

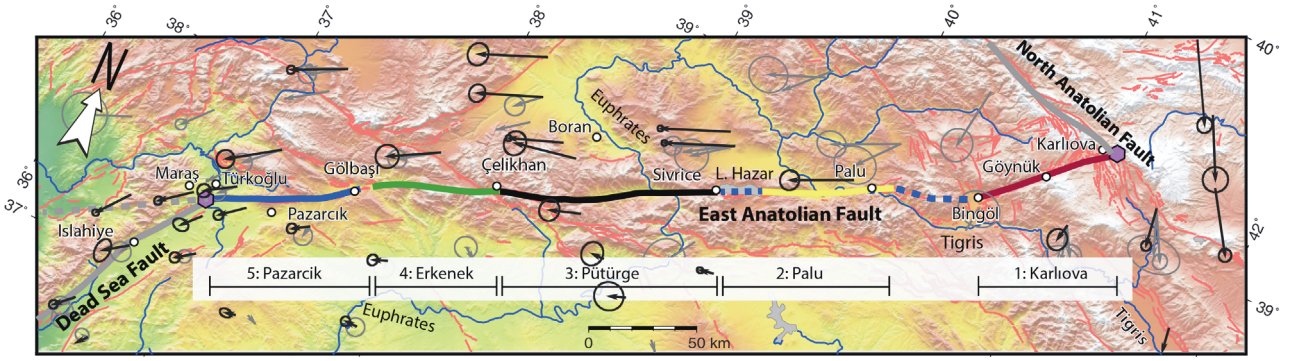

Figure 2. Segmentation of the East Anatolian Fault following Duman and Emre (2013); active faults are from Emre et al. (2013). Purple hexagons indicate the location of the Karlıova and Maraş triple junctions. Blue lines show the main rivers and streams (e.g., Euphrates River).

Segment 2 (Palu) stretches for 77 km. The last historical earthquake on this segment occurred on 3 May 1874 with M_w of 7.1 (Ambraseys, 1988; Ambraseys and Jackson, 1998) (Figure 3b). The human damage was greatest between Lake Hazar and Palu (Ambraseys, 1988). East of Lake Hazar, Herece (2008) reported a 2.6-m-lateral offset along the rupture zone, and Duman and Emre (2013) suggested the average displacement of the 1874 earthquake to be 3.5 ± 0.5 m in the central part of the Palu segment. The Lake Hazar basin sits astride the active trace of the EAF, and the basin is bounded by normal faults to the north and south (Moreno et al., 2010).

The EAF traverses mountains terrain and follows linear valleys along segment 3 (Pütürge; Figure 3c), where it cuts Paleozoic-Mesozoic metamorphic and Mesozoic ophiolite mélange and volcanosedimentary rocks (Hempton, 1985; Herece and Akay, 1992; Herece, 2008). Ambraseys (1988) suggested that the 1875 (M_w 6.8) and 1905 (M_w 6.9) earthquakes were generated along this segment.

Segment 4 (Erkenek) extends northwards from Lake Gölbaşı. This segment is characterized by late Pleistocene and Holocene left-lateral displaced streams with offsets ranging from several meters to 500 m (Duman and Emre, 2013). One particular stream, the Göksu River, is offset by ~13 km (Şaroğlu et al., 1992a, 1992b) (Figure 3d), which yields a Quaternary slip rate of ~6.5–8.3 mm/year (Herece, 2008; Duman and Emre, 2013). The northern margin of the Gölbaşı basin is bounded by normal faults. These faults are relatively short (3–10 km in length), discontinuous, and slightly curved and dip to the south trending N72°E within a 3-km-wide zone (Duman and Emre, 2013). Varying geologic offsets have been recorded that range from 19 to 26 km. Several fault-related basins, e.g., the Hazar and Gölbaşı basins, are present along segment 4. The Gölbaşı basin is the largest basin along the EAF (Yönlü et al., 2013). Yönlü et al. (2013) examined the geology and geomorphology around the Gölbaşı basin and argued that there was a wide river valley in which the Aksu River flowed and was later blocked by a landslide at 31.6 ± 0.5 ka. They concluded that as a result of this obstacle, the Aksu River changed its course and was left laterally offset by the EAF by ~16.5 ± 0.5 km. This is the largest recorded geomorphic offset along the EAF.

A Holocene slip rate of 9 mm/year has been determined using tectonics and GPS measurements along segment 5 (Pazarcık) (Yalçın, 1979; Meghraoui et al., 2006; Westaway et al., 2006; Herece, 2008; Karabacak et al., 2011) (Figure 3e). Yönlü et al. (2012) suggested a 5 ± 0.5 mm/year slip rate for the Pazarcık segment based on the paleoseismological data. Duman and Emre (2013) suggested that the surface ruptures on segment 5 are due to the AD 1114 and 1513 earthquakes. This segment of the EAF includes the Gölbaşı basin that formed in a releasing step-over and is marked by a 15° change in the dominant fault trace.

4. Methodology

ArcGIS software and a 30-m resolution digital elevation model (DEM) extracted from a Shuttle Radar Topography Mission (SRTM) were used for topographic analysis along the entire length of the EAF (Farr et al., 2007). Geomorphic indices were applied along the EAF within a zone of ~30 km on both sides of the fault trace. The hill-shade option in ArcGIS was used to analyze the mountain-front sinuosity. Hydrology and raster calculation tools were used to construct and classify catchments that had stream greater than the fourth order using the stream order scheme of Strahler (1952) (Figure 4). The catchments, watershed delineation, catchments sizes, and river drainage pattern were extracted from the digital elevation data using algorithms available in the hydrology toolbox of ArcGIS. The catchments were numbered from 1 to 18 from east to west (Figure 4). The resolution of the DEM limited the degree of uncertainty associated with the geomorphic indices. We do not assign an uncertainty to our geomorphic indices as in other studies (e.g., El Hamdouni et al., 2008; Tari and Tüysüz, 2015).

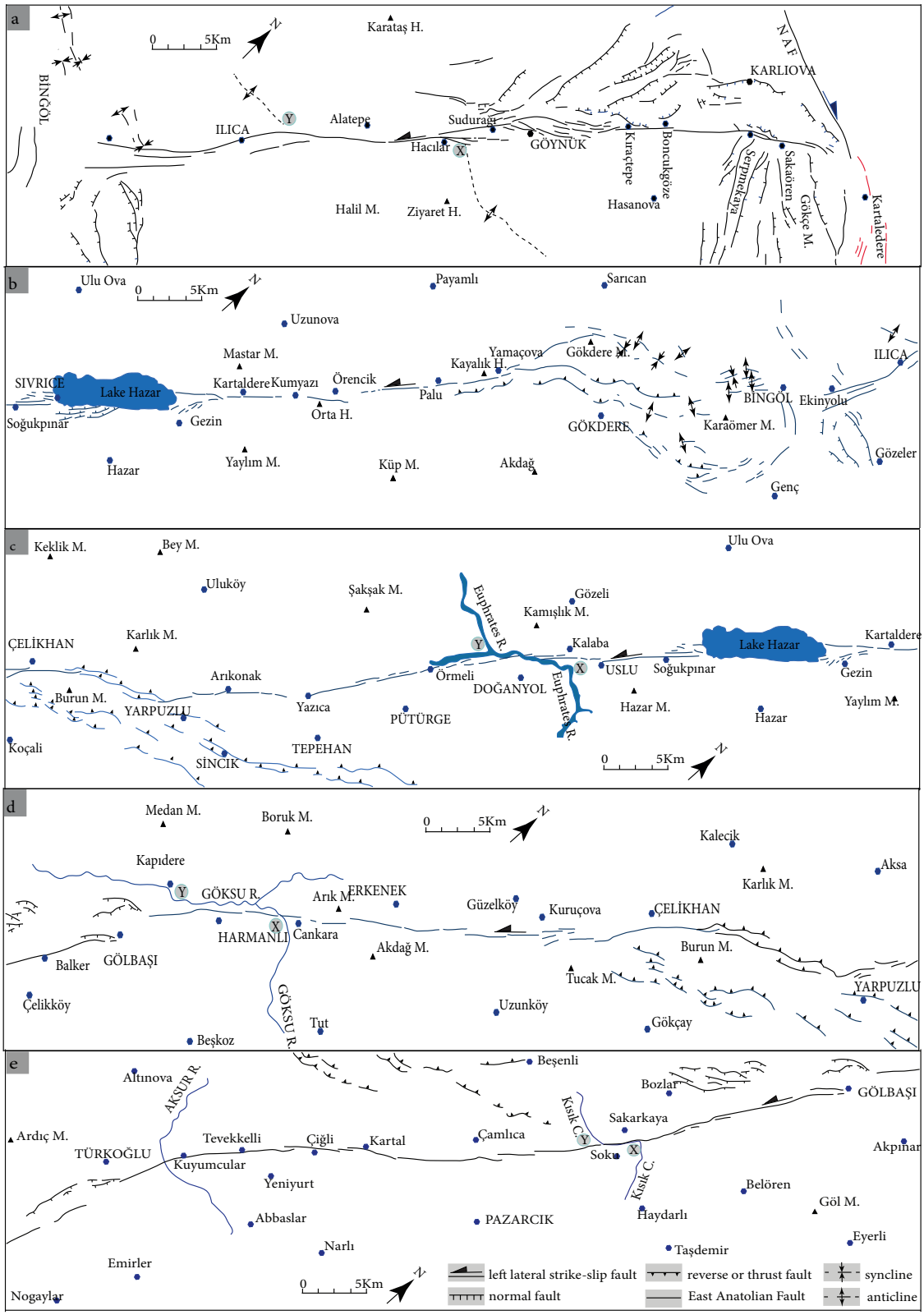

Figure 3. Details of segments 1 through 5 along the EAF: (a) 1- Karlıova, (b) 2- Palu, (c) 3- Pütürge, (d) 4- Erkenek, and (e) 5- Pazarcık segments of the East Anatolian Fault modified after Duman and Emre (2013). NAF, North Anatolian Fault; M, mountain; H, hill; C, creek; 'x' and 'y' denote piercing points.

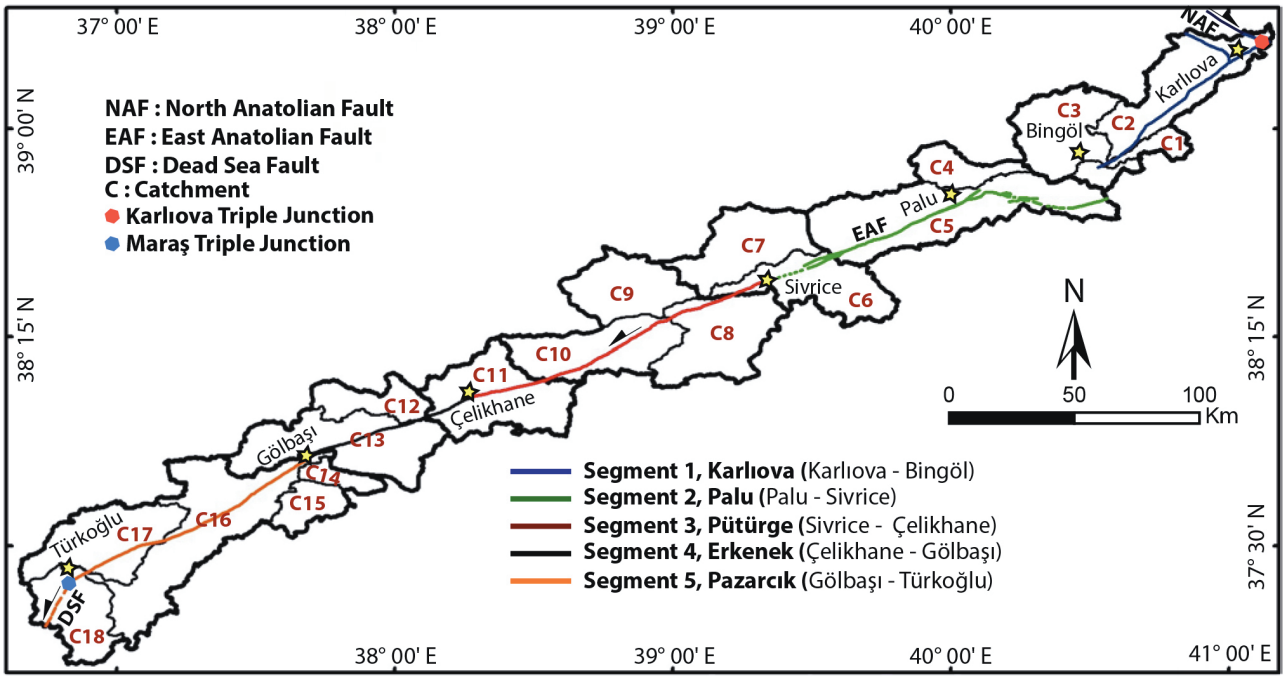

Figure 4. Studied catchments along the East Anatolian Fault Zone.

4.1. Geomorphic indices

4.1.1. Rock strength

The aim of our study was to evaluate the morphotectonic indices of the fault depending on the rocks' strength along the mountain front of the fault deformation zone and recognize the rock resistance based on geological maps, field observations, and similar papers (e.g., El Hamdouni et al., 2008; Alipoor et al., 2011; Selçuk, 2016). We consider rock hardness as Selby (1980) did, with strength related to the constituent material and cement assisting in the resistance to weathering and erosion processing. Rock strength is classified as very low (silt, sand, marl, alluvium, limestone), low (conglomerate, sandstone, shale with interbedded limestone), medium (sandy limestone), high (basalt), or very high (gneiss, schist, gabbro, marble, quartzite).

4.1.2. Stream length-gradient index (S_L)

The S_L index is sensitive to channel slope, which, in turn, can be used as a proxy for tectonic activity, stream power, and/or rock resistance. Erosional resistance of rocks and relative intensity of active tectonics can be evaluated using S_L by calculating changes of stream gradients along drainage catchments (Hack, 1973; Keller and Pinter, 2002). The S_L index is defined as:

$$S_L = (\Delta H / \Delta L) \times L, \quad (1)$$

where $\Delta H/\Delta L$ is the channel gradient for a stretch of the stream (ΔH is the elevation change for a particular channel reach with respect to ΔL, i.e. the length of the reach) and the total channel length L from the midpoint of the reach where the index is calculated upstream of the drainage divide. The S_L index is generally calculated for a large number of reaches along major streams within a study area (Azor et al., 2002). S_L values were calculated every 100 m along the length of the main stream channels of the EAF.

4.1.3. Mountain-front sinuosity (S_{mf})

S_{mf} helps define the relationship between the total length and the straight-line distance along a mountain front (Bull, 1977; Azor et al., 2002; Keller and Pinter, 2002). This index helps explore links between tectonics and erosion, and it is defined as:

$$S_{mf} = L_{mf} / L_s, \quad (2)$$

where L_{mf} is the length of the mountain front and L_s is its straight-line length. S_{mf} values were calculated for 18 mountain fronts along the 5 segments of the EAF from the SRTM 30-m pixel-resolution DEM. S_{mf} values approaching 1 suggest a more active tectonic setting.

4.1.4. Valley width to height ratio (V_f)

V_f defines the differences in valley shape and may reflect the degree of active uplift and/or base level fall, and it is defined as:

$$V_f = 2V_{fw} / [(E_{ld} - E_{sc}) + (E_{rd} - E_{sc})], \quad (3)$$

where V_{fw} is the width of the valley floor, E_{rd} and E_{ld} are respectively the elevations of the right and left valley divides, and E_{sc} is the average elevation of the valley floor (Keller and Pinter, 2002).

Azor et al. (2002) suggested that high values of V_f usually indicate low tectonic activity, whereas low values

indicate areas of high tectonic activity with relatively rapid uplift and valley incision. V_f values were calculated at a prescribed distance (1 to 3 km) from the mountain front based on the size of the drainage regions (Silva et al., 2003). V_f values were determined for 77 streams aligned along the mountain fronts of the EAF.

4.1.5. Basin asymmetry factor (A_F)

A_F may be utilized to help detect tectonic tilting from drainages that transverse a structure and is defined as:

$$A_F = 100 (Ar / At), \quad (4)$$

where Ar is the area of the drainage basin to the right of the main stream and At is the total area of the basin. A_F is sensitive to tilting perpendicular to the trend of the main stream. An A_F of 50 represents a tectonically stable setting, while values smaller or greater than 50 suggest tilting and indicate that a basin is tectonically active (Keller and Pinter, 2002). Values of A_F include the A_F-50, which is the difference amount between the neutral value of 50 and the observed value (El Hamdouni, 2008). An absolute difference (difference from an A_F of 50) is necessary to evaluate the relative tectonic activity. We categorize the absolute values of A_F into class 1 ($|A_F\text{-}50| > 15$), class 2 ($|A_F\text{-}50|$: 7–15), and class 3 ($|A_F\text{-}50| < 7$) following the method of El Hamdouni (2008). El Hamdouni (2008) classified the average of the different classes into four activity levels, where level 1 is very high relative tectonic activity (1 to 1.5), level 2 indicates highly relative tectonic activity (>1.5 to ≤2), level 3 is moderately relative active tectonics (>2 to ≤2.5), and level 4 is the lowest level of relative tectonics (>2.5). A_F values were calculated for the 18 catchments along the EAF.

4.1.6. Drainage density (D_d)

Azor et al. (2002) and Keller and Pinter (2002) introduced D_d as the ratio of total channel length versus catchment area. Greater values of D_d suggest more extensively developed regions for a relatively long time, while regions experiencing the most recent tectonic activity have lower D_d values (Keller and Pinter, 2002). D_d is defined as:

$$D_d = L / A , \quad (5)$$

where L is the length of the channel and A is the catchment area. D_d was defined along the EAF throughout 18 catchments.

4.1.7. Hypsometry

The hypsometric integral (H_i) is a quantitative measure of the distribution of elevation within a catchment (Langbein, 1947; Strahler, 1952). This index serves to compare catchments and is an expression of the volume of the catchment that has not been eroded. Simply expressed, the H_i index (Pike and Wilson, 1971; Mayer, 1990) is defined as:

$$H_i = (E_{mean} - E_{min}) / (E_{max} - E_{min}), \quad (6)$$

where E_{mean} is the mean elevation, E_{max} is the maximum elevation, and E_{min} is the minimum elevation.

The hypsometric curve of a catchment is the cumulative area versus elevation plot, which likely reflects the dominant geomorphic processes operating in the catchment. A convex curve indicates uplift with dominant hillslope processes, such as sliding and soil creep, while a concave curve indicates channelized/linear/fluvial/alluvial processes. In essence, young catchments (tectonically active) have H_i values of ≥0.45 and convex hypsometric curves, whereas low H_i values (≤0.3) and concave hypsometric curves indicate old catchments (tectonically quiescent). H_i values were calculated for 18 catchments along the EAF.

5. Results

5.1. Rock strength

The mountain front along the EAF consists of large varieties of rocks. The geological units of the studied catchments comprise basalt, volcanic rocks, gabbro-diabase, carbonate rocks, marble, gneiss and schist, neritic limestone, and undifferentiated Quaternary rock and sediment (Figure 5a) that imply the presence of all rock strength levels. This, in turn, minimizes the effect of lithology on the calculated morphometric indices. Very high and low strength rocks mostly are exposed along segment 3. Segments 1 and 4 include high and moderate rock strengths. The mountain fronts along segments 1, 2, and 5 are made up of moderate, low, and very low strength of rocks. In the central part of the EAF, segments 3 and 4 comprise rocks with high rock strengths (Figure 5b).

5.2. Stream length-gradient index (S_L)

S_L values range from 50 to 350 along the stream channels of the fault zone (Figure 5b). The lowest index values are along the upstream reaches of the drainage catchments, while the highest values are located across the mountain fronts. The S_L values show some low values when flowing parallel to the valleys that were likely produced by the fault. S_L values increase toward the mountain fronts (Figure 5b). The highest values of the index are also recorded in most catchments that are not associated with particularly resistant rocks. Anomalous values of the S_L index are noticed along the five segments.

5.3. Mountain-front sinuosity (S_{mf})

The five segments, from east to west, have S_{mf} values of 1.07–1.17, 1.05–1.46, 1.06–1.09, 1.01–1.09, and 1.07–1.28 (Figure 6; Table 1). The lowest S_{mf} values are associated with segments 3 and 4, while the highest values are for segment 2. The S_{mf} values show that each segment reflects topographic signals of active uplift and all fault segments are active along the EAF. On the basis of the similar S_{mf} values there is no obvious change in tectonic activity along the EAF.

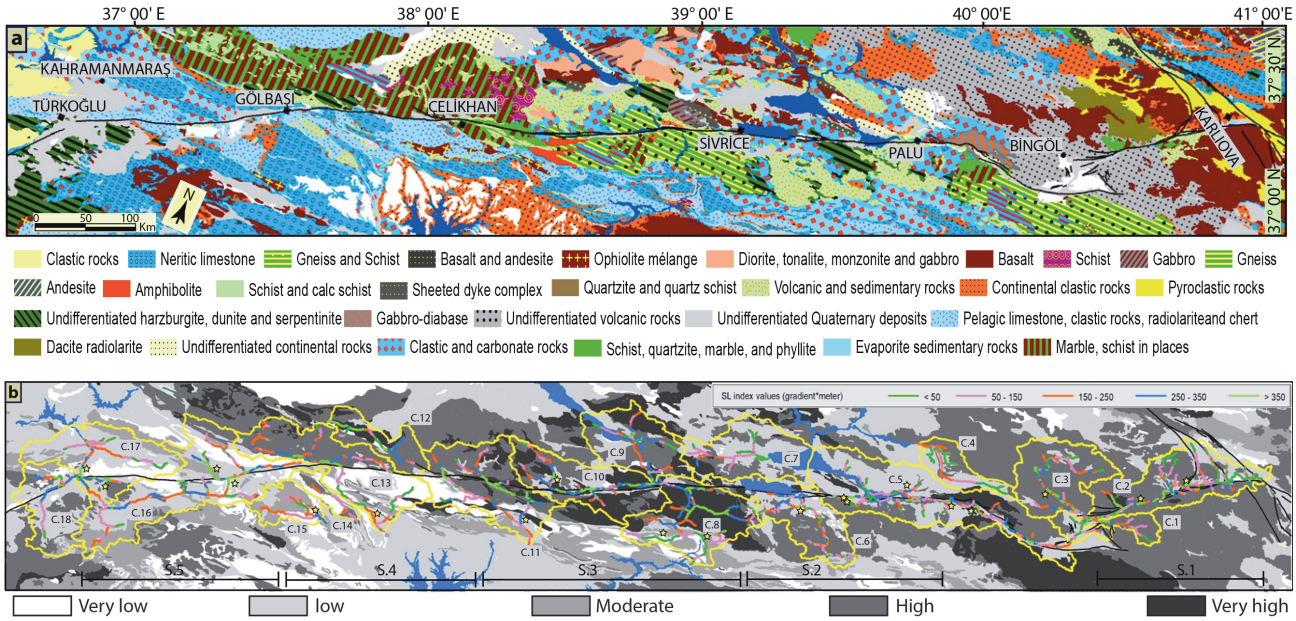

Figure 5. (a) Geological map of the EAF (extracted from the geological maps catalogue of the General Directorate of Mineral Research and Exploration of Turkey), (b) SL index along the channels and rock strength level (according to El Hamdouni, 2008) of the studied fault. Yellow stars indicate the distribution of the SL index anomalies.

5.4. Valley width to valley height ratio (V_f)

The V_f index is calculated for the main valleys and streams that cross and run parallel to the mountain fronts of the studied zone (Figure 6). V_f values vary depending on rock type, stream discharge, and catchments sizes. From east to west, mean V_f values are 0.47–0.75, 0.61–1.32, 0.24–0.61, 0.11–0.37, and 0.54–0.80 for the five segments (Figure 6; Table 1). The lowest mean values are for segment 4, while the highest values are for segment 2. The results suggest a general similarity between S_{mf} and mean V_f values of the five segments. The V_f values' consistency with S_{mf} might give a good signal to evaluate the tectonic activity of the segments.

5.5. Basin asymmetry factor (A_F)

A_F-50 values range from 1.88 to 26.25, which indicates the differences between the observed value of 50 and the neutral value (Table 2). The results show that catchments 7, 4, and 17 have values close to 50 and the catchments that have the highest values away from 50 are 2 and 15 (Table 2). Within the study area, A_F index classes were applied to record class 1 of the relative tectonic activity for catchments 2, 8, 9, 11, 13, 15, and 16; class 2 was examined for catchments 3, 6, 10, 12, 14, and 18; and relative tectonic activity class 3 was measured for catchments 1, 4, 5, 7, and 17 (Table 2).

5.6. Drainage density (D_d)

D_d varies from 3.5 to 5.6 km/km^2 (Table 2). Catchment 4 has the highest D_d, while the lowest values are for catchments 11 and 13. The catchments in general have a remarkably low D_d, and most drainages reflect deep incision. The average D_d of the catchments is low in segments 3 and 4.

5.7. Hypsometry (H_i)

H_i values range from 0.25 to 0.58. High values of the H_i index are recorded for catchments 8 and 7, which generally indicate that not as much of the uplands have been eroded and suggests younger catchments and landscape, most probably created under active tectonics conditions. Catchment 2 has the lowest H_i values, which is probably due to a relatively older landscape with more erosion and less subjected by recent active uplifting. The hypsometric index data suggest that the middle part of the EAF is slightly more active than the rest of the fault and has the youngest catchments, albeit only slightly younger. Similarly, H_i curves recorded (1) convex curves in catchments 11, 12, 13, and 16; (2) concave-convex or slight curves in catchments 1, 2, 3, 5, 6, 7, 9, 10, 14, 15, 17, and 18; and (3) concave curves for catchments 2 and 5 (Figure 7).

5.8. Average of the geomorphic indices

The mean S_{mf}, V_f, and D_d values gradually increase from segment 4, 3, 1, and 5 to 2 (Table 3). Segments 3 and 4 have level 1 relative tectonic activity, while segments 1 and 5 have level 2 relative tectonic activity and segment 2 has a relative tectonic activity level of 4 (Table 3). H_i values gradually decrease from segment 4, 3, 5, and 1 to 2 (Table 3).

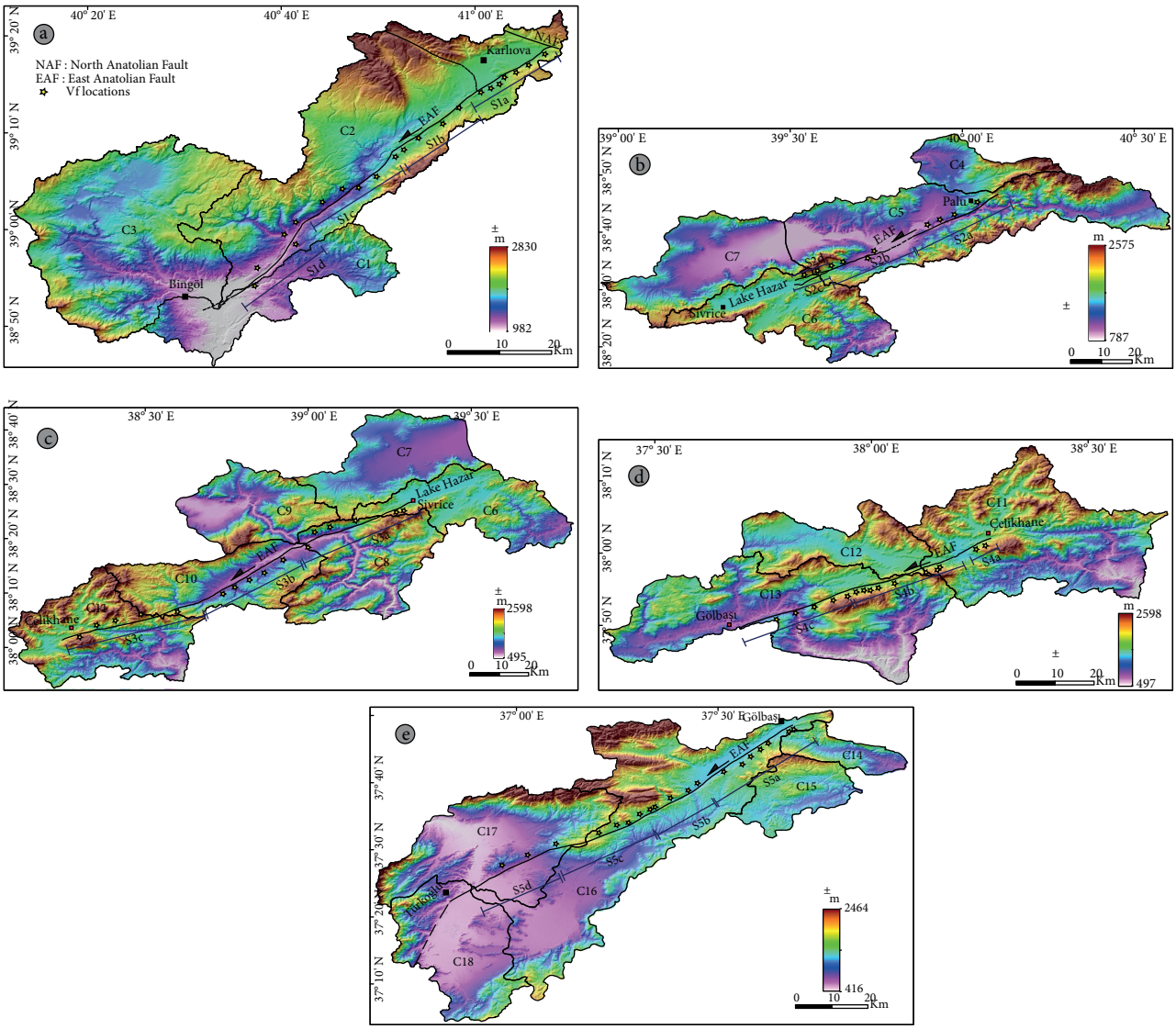

Figure 6. (a) Karlıova (b), Palu (c), Pütürge (d) Erkenek, (e) Pazarcık segments on top of colored shaded elevation image.

6. Discussion

6.1. Relative tectonic activity based on geomorphic indices

Many studies have used the combination of indices S_{mf} and V_f to present a preliminary overview of the relative tectonic activity of the fault mountain fronts (Bull and McFadden, 1977; Silva et al., 2003; Yıldırım, 2014). In our study, there is general uniformity between S_{mf} values and V_f mean values of the five fault segments along the EAF. Our S_{mf} values suggest that all fault segments are young and active along the fault, and that each segment is likely undergoing tectonic uplift. The highest value of S_{mf} (low tectonic activity) is associated with segment 2, while the lowest values are for segments 4 and 3 (high tectonic activity), which indicates a straighter mountain front than the others. The highest degree of tectonic uplift occurs in segment 4 and this is consistent with the view of Yönlü et al. (2013), who discussed the presence of the largest morphological offset of the EAF along the same segment.

V_f values suggest continued and comparatively high uplift rates along the EAF. Lower values in the central valleys suggest a higher uplift and incision rate than in the southern and northern parts of the EAF. Keller and Pinter (2002) suggested that S_{mf} values of 1.0–1.6 are indicative of active range-bounding fault zones. Some studies, e.g., those of Bull and McFadden (1977) and Rockwell et al. (1984), constructed a diagram for the S_{mf} and V_f values, showing the distribution of these index values along streams and mountain fronts (Figure 8). They plotted the S_{mf} with V_f values in the same diagram to classify relative

Table 1. Values of the mountain-front sinuosity and valley floor width to height ratio of measurements (see locations in Figure 4).

Mountain front	S_{mf}	V_f (mean)
S1a	1.08	0.74
S1b	1.17	0.75
S1c	1.07	0.47
S1d	1.13	0.65
S2a	1.39	0.61
S2b	1.44	1.32
S2c	1.46	0.64
S2d	1.05	0.64
S3a	1.08	0.30
S3b	1.09	0.61
S3c	1.06	0.24
S4a	1.09	0.11
S4b	1.01	0.21
S4c	1.03	0.14
S4d	1.04	0.37
S5a	1.28	0.80
S5b	1.15	0.54
S5c	1.07	0.75
S5d	1.08	0.67

tectonic activity into 3 classes and detect a relative tectonic activity degree. S_{mf} versus V_f plots show that all segments are indicative of the highest tectonic activity, i.e. Class I (Figure 8). Class 1 is commonly associated with uplift rates between 0.05 and 0.5 mm/year (e.g., Rockwell et al., 1984; Yıldırım, 2014). Although all the EAF segments are plotted as a higher activity class, they reveal differences in relative tectonic activity values. From high to low, these are segment 4, 3, 1, 5, and 2. The results show slight differences and nearly uniform values of S_{mf} along the entire fault, implying that the tectonic activity along the whole EAF zone is nearly the same. This is also consistent with the published uniform slip rate of ~10 mm/year along the whole EAF based on GPS measurements (Reilinger et al., 2006; Mahmoud et al., 2013; Aktuğ et al., 2016). The S_L values over the study region calculated from the DEM and GIS software are shown in Figure 5b, which illustrates the relationship between S_L values and the underlying geology. Over most of the studied catchments rivers, the S_L values increase abruptly in the same rock type (Figure 5b), except rivers over catchment 5. Over this catchment the rock strength changes alternately from very low to moderate, where S_L values of catchment streams increase. In such a case, Yıldırım (2014) argued that the effect of the rock strength is small on the increase of values of S_L in the same rock strength along the rivers. El Homdouni et al. (2008), Alipoor et al. (2011), and Azañón et al. (2012) presented anomalous values of the S_L index for the high S_L values that are not associated with resistant rocks and they interpreted these anomalous values as tectonic signals. Within our study zone, anomalous measurements are recorded along nearly all segments, which reflects high uplifting activities. The S_L results are also greater on both sides of the fault, which indicates recent and continued uplift along the EAF. In our study, S_L values increase abruptly in the same rock units and we detected many anomalous spots along all segments that likely reflect tectonic signals. In addition to the previous remarks, we found that nearly all catchments have the same varieties of rock strength types. Based on these conditions, we assume that the impact of the geology is negligible and tectonic impact is prevailing. Based on the uniformity of the climatic conditions along the whole fault zone, the S_L index results that generally reflect both rock strength and climate and drainage development and local geomorphology that are affected by the tectonic uplifting and regional deformation suggest that climate does not have a highly significant impact on the studied deformation zone.

The A_F factor is sensitive to change in catchment inclination perpendicular to the mean channel direction (El Hamdouni et al., 2008). Structural control of the bedding orientation may play a great role in the development of basin asymmetry (Alipoor et al., 2011). Except for catchments 1, 4, 5, 7, and 17 (tectonically more stable), the A_F values for all catchments indicate tilting and relative active tilting/uplifting. Catchments 2, 5, and 12 are located in the studied deformation zone but they are still away from the EAF fault trace. According to El Hamdouni (2008), the mean values of A_F differentiate the segments into three levels of tectonic activity. Segments 3 and 4 were defined by the first level of the relative tectonic uplifting that reflects the highest tectonic activity, segments 1 and 5 show the second level of uplifting, and the third level that reflects the lowest degree of tectonic uplifting was recorded for only segment 2.

Values of D_d help define the degree to which drainage development has dissected a structural landform (Melosh and Keller, 2013). Topal et al. (2016) assumed that low D_d values characterize drainages that are nearly straight and have steep channels that characterized the catchments with recent movement activity. Catchments 4, 5, 14, and 15 are located away from the fault trace and likely have less tectonic uplift than the other catchments that have lower D_d values. Overall, segment 4 has the lowest D_d value and reflects relatively higher uplift than segment 2 that has the highest D_d value. H_i does not relate directly to relative active tectonics (El Hamdouni et al., 2008). H_i values are affected by the rock strength

Table 2. Asymmetry factor (A_F), drainage density (D_d), and hypsometric integral (H_i) of the different catchments of the study area.

Catchments	A_F	A_F-50	A_F (Class)	D_d	H_i
C1	44.76	−5.24	3	4.1	0.45
C2	76.25	26.25	1	4.5	0.48
C3	59.93	9.93	2	4.7	0.47
C4	47.73	−2.27	3	5.6	0.27
C5	54.29	4.29	3	4.9	0.33
C6	57.82	7.82	2	4.8	0.36
C7	48.12	−1.88	3	4.6	0.25
C8	66.83	16.83	1	4.2	0.54
C9	67.88	17.88	1	3.9	0.45
C10	58.67	8.67	2	4.1	0.48
C11	66.39	16.39	1	3.5	0.56
C12	44.14	−5.86	2	4.3	0.51
C13	28.04	−21.96	1	3.8	0.58
C14	59.90	9.90	2	5.0	0.41
C15	70.00	20.00	1	4.9	0.45
C16	32.28	−17.72	1	4.3	0.53
C17	53.80	3.80	3	4.1	0.40
C18	37.85	−12.15	2	4.0	0.46

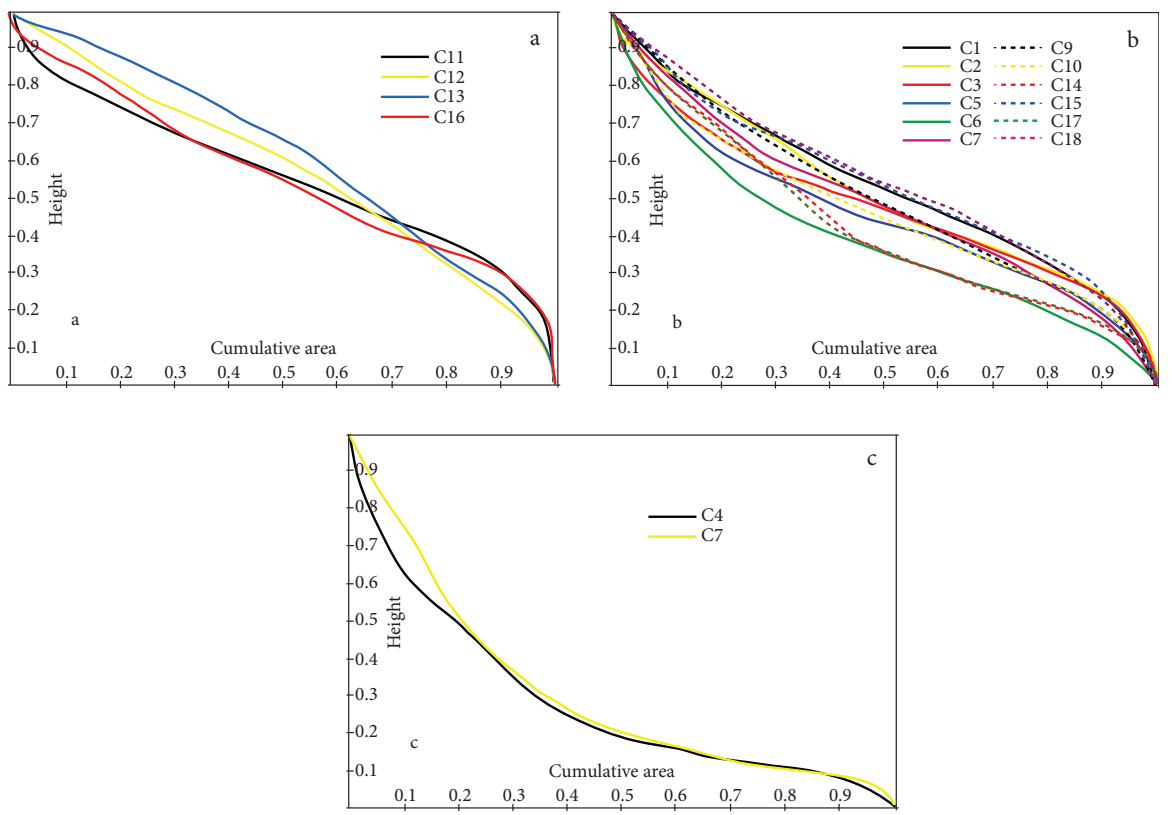

Figure 7. Hypsometry curves of 18 catchments along the EAF shown in Figure 4. (a) Convex hypsometric catchments (weakly eroded catchments), (b) convex-concave hypsometric catchments (moderately eroded catchments), and (c) concave hypsometric catchments highly eroded catchments).

Table 3. Mean morphometric parameters of the studied segments and catchments.

Segments	S_{mf}	V_f	Catchments	Mean A_F (class)	A_F activity degree	Mean D_d	Mean H_i
Segment 1	1.11	0.67	C1, C2, and C3	2.00	2	4.43	0.46
Segment 2	1.34	0.75	C4, C5, C6, and C7	2.75	4	4.97	0.31
Segment 3	1.07	0.38	C6, C8, C9, C10, and C11	1.40	1	4.12	0.48
Segment 4	1.04	0.21	C11, C12, and C13	1.30	1	3.86	0.55
Segment 5	1.15	0.74	C14, C15, C16, C17, and C18	1.80	2	4.47	0.45

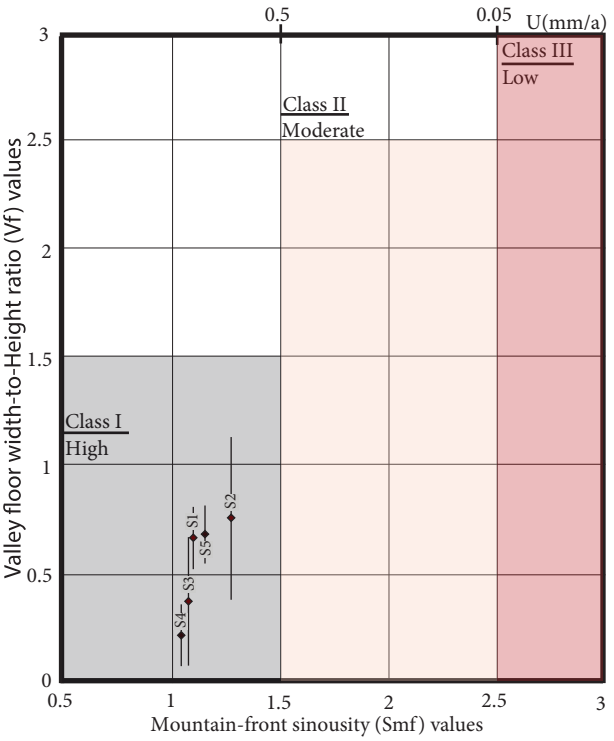

Figure 8. Plot of S_{mf} versus V_f for the mountain fronts of each segment and inferred activity classes. Vertical bars show the standard deviation for V_f values. Numbers at the top indicate inferred uplift rates U (mm/year) from Rockwell et al. (1984).

(El Hamdouni et al., 2008). H_i index values that indicate high tectonic uplift rates and are characterized by convex curves are evident for catchments in segments 3 and 4, while H_i values show a low rate of tectonic uplifting with concave curves in catchments 4 and 7, which are located away from the fault trace (Figure 7; Table 2).

Average values of H_i decrease gradually from segments 4, 3, 1, and 5 to 2 (Table 3). The results suggest that all the catchments along segments 4 and 3 are young and have relatively high rates of uplift compare to the other segments.

In conclusion, the geomorphic indices suggest that all the segments along the EAF are highly active (class 1) and have similar uplift rates. The catchments that are away from the EAF show intermediate to low degrees of tectonic activity and that reflects the rate of uplifting and tectonic decreases away from the fault trace.

6.2. Implications of long-term deformation patterns

The EAF accommodates most of the relative movement of the Arabian and Anatolian plates (Duman and Emre, 2013). Variations of the S_{mf} and V_f, indices (Figures 8 and 9a) and values of the S_L, A_F, D_d, and H_i indices (Table 3) provide a means to help examine variations of tectonic uplifting activity along the fault (Yıldırım, 2014).

Although values for all geomorphic indices along the fault segments are different, they are mostly of the same activity zone (Figures 9a–9c), implying that all the segments have comparable tectonic activity and have undergone similar amounts of erosion over time. The uniform variation in geomorphic indices might also indicate that either all the fault segments were initiated at the same time and underwent similar morphological evolution or some fault segments formed later, but experienced higher erosional rates. The former possibility of geomorphic indices' uniformity appears to be more likely considering the relatively uniform total offset of 13–30 km and the uniform and constant slip rate of ~10 mm/year along the entire fault (Reilinger et al., 2006; Mahmoud et al., 2013; Aktuğ et al., 2016). In contrast, the cumulative offset along the NAF becomes smaller and the width of the shear zone gets wider from east to west (Şengör et al., 2014). This is because the NAF becomes younger to the west as it has propagated westward at a rate of ~11 cm/year (Şengör et al., 2004).

Dewey et al. (1986) and Westaway and Arger (1996) suggested that the EAF is a root of the distributed deformation and is oblique to the assumed Anatolian/Arabian plate motion, and as such the EAF is not a true transform fault. In contrast, Westaway (1994a) concluded that the Anatolian/Arabian plate boundary is a real transform fault system since it initiation at ~5 Ma. He

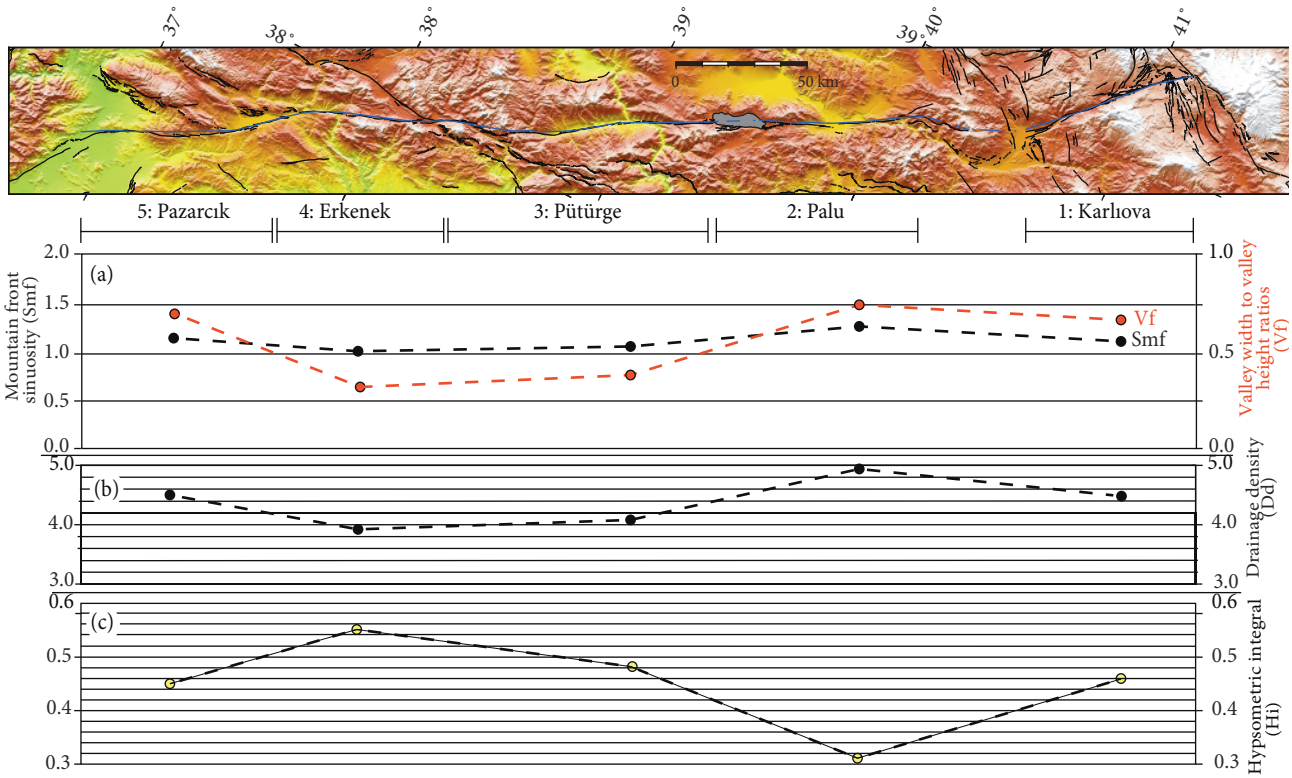

Figure 9. Morphometric indices (a–c) along the East Anatolian Fault. S_{mf}, Mountain front sinuosity; V_f, valley width to valley height ratios; (D_d) drainage density; H_i, hypsometric integral.

argued that since ~5 Ma, the MOFZ that is subparallel to the EAF has taken up part of the Anatolian/Arabian plate movement. Arger et al. (1996) and Westaway and Arger (1996) recorded evidence that the MOFZ is presently inactive and proposed instead a scheme where the Anatolian/Arabian plate boundary was formed by the MOFZ from ~5 to 3 Ma and the EAF has created this boundary since ~3 Ma (Figure 10). Westaway (1994) argued that the MOFZ and EAF are tectonically equivalent, and both have taken up the ~70 km of the estimated Anatolian/Arabian boundary since ~5 Ma. In contrast, Westaway and Arger (1996) argued that the MOFZ created the African/Anatolian plate boundary since 3–5 Ma and no significant slip has occurred since that time. This is based on: (1) the lack of recorded seismicity, (2) the field work of Westaway and Arger (1996) that does not show any geomorphic evidence for recent slip, and (3) the fact that if the western and eastern areas of Erzincan and the MOFZ are active at the same time, very intense deformation would be recorded around their intersection region, which has not been recognized. Westaway and Arger (1996), therefore, concluded that the MOFZ was the Anatolian/Arabian plate boundary at ~5 Ma and later. This boundary moved southeast to occupy its modern location at ~3 Ma. In contrast, some researchers, e.g., Koçyiğit and Beyhan (1998) and Kaymakcı et al. (2006), suggested a different hypothesis for activity along the MOFZ. They argued that the MOFZ is tectonically active at present and it is a part of the present motion between the Anatolian/Arabian plates. Westaway and Arger (2001) argued against the view of Koçyiğit and Beyhan (1998) because they did not offer any quantitative examinations of the kinematics of the MOFZ to support their different scenarios. As discussed above, our geomorphic analysis suggests coeval development along the different segments of the EAF and supports the view of an eastward jump of the proto-EAF (~110 km) from what is now the MOFZ to its present-day EAF at ~3 Ma (Figure 10; Arger et al., 1996; Hubert-Ferrari et al, 2009). Westaway (1994a) calculated a convergence rate of 14 ± 2 mm/a for the Anatolian/Arabian plate, which since initiation of slip on the EAF zone has accommodated ~30 km of convergence, with all the 14 ± 2 mm/a slip occurring on the MOFZ. Before initiation of slip on the EAF, the NAF ended at Erzincan and its present eastern stretch did not exist (Figure 10).

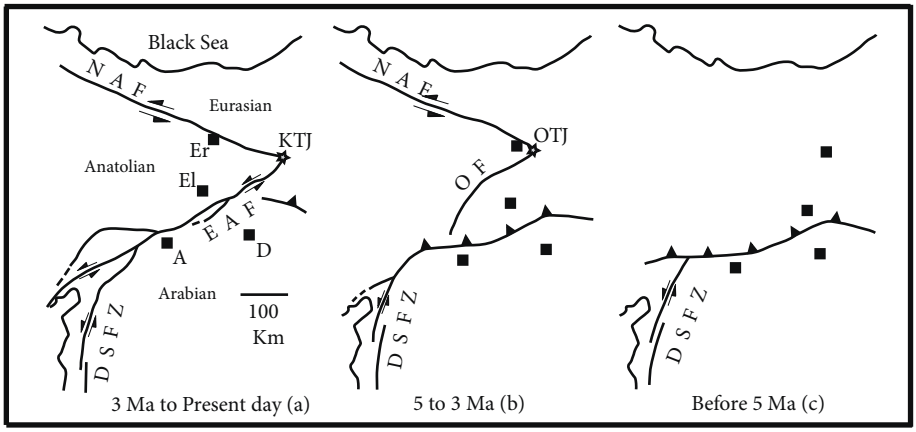

Figure 10. Summary of the evolution of the triple junction between the Arabian, Eurasian, and Anatolian plates (from Arger et al., 1996; Westaway and Arger, 1996, 2001; Hubert-Ferrari et al., 2009). OTJ, Ovacık triple junction; KTJ, Karlıova triple junction; OF, Ovacık Fault; Er, Erzincan; El, Elazığ; D, Diyarbakır; A, Adıyaman. (a) Present day. (b) Immediately before the modern fault geometry developed between 3 and 5 Ma. (c) Immediately before change in plate geometry at 5 Ma.

7. Conclusions

Geomorphic indices, including S_L, S_{mf}, V_f, A_F, D_d, and H_i, are used for the first time along the EAF to gain deeper insights into morphotectonic evolution and activity of the EAF. S_{mf} versus V_f values are positively correlated and indicate a high degree of tectonic and geomorphic activity, which is also supported by the results from stream gradient analysis and hypsometric analysis. This implies that each segment along the fault is presently very active.

The similar values for geomorphic indices along the entire length of the fault suggests that the development of the EAF was essentially coeval along its length, supporting the view that the present-day Anatolian/Arabian plate boundary, i.e. the EAF, jumped eastward from the MOFZ from the proto-EAF to its present-day location at ~3 Ma. This is in good agreement with the nearly uniform geological offsets and the present day slip rate of ~10 mm/year along the entire fault that appears to have been constant since ~3 Ma.

This study illustrates that morphometric analysis along the entire length of a major strike-slip fault provides important insights into the fault's tectonic evolution. Calculations of multiple catchments' geomorphic indices and indices that are related to the trace of the faults can provide us with valuable data on the tectonic behaviors and landscape evolution. Thus, this can be applied to other major faults elsewhere, especially to those whose tectonic activity, cumulative offset, and slip rates are not well defined.

Acknowledgments

This work was supported by İstanbul Technical University with a Scientific Research Projects Unit project. The PhD scholarship to the first author by the Turkish Government is acknowledged. The authors are thankful to Cengiz Yıldırım, İstanbul Technical University, for his suggestions and significant discussion to improve our work. We also like to thank Elizabeth Orr, University of Cincinnati, for critical reading of the manuscript. The authors are grateful to manuscript editor Dr Taylan Sançar for his comments and judicious evaluation that significantly improved the manuscript. The considerable improvement of our manuscript by Dr Savaş Topal and the other two anonymous referees' comments, remarks, and recommendations are gratefully acknowledged.

References

Aksoy E, İnceöz M, Koçyiğit A (2007). Lake Hazar Basin: a negative flower structure on the East Anatolian Fault System (EAFS), SE Turkey. Turkish J Earth Sci 16: 319-338.

Aktuğ B, Özener H, Dogru A, Sabuncu A, Turgut B, Halicioglu K, Yilmaz O, Havazli E (2016). Slip rates and seismic potential on the East Anatolian Fault System using an improved GPS velocity field. J Geodynamics 94-95: 1-12.

Alipoor R, Poorkermani M, Zare M, El Hamdouni R (2011). Active tectonic assessment around Rudbar Lorestan dam site, High Zagros Belt (SW of Iran). Geomorphology 128: 1-14.

Allen CR (1969). Active Faulting in Northern Turkey. Pasadena, CA, USA: Division of Geological Sciences, California Institute of Technology.

Ambraseys NN (1988). Temporary seismic quiescence: SE Turkey. Geophys J Int 96: 311-331.

Ambraseys NN, Jackson JA (1998). Faulting associated with historical and recent earthquakes in the Eastern Mediterranean region. Geophys J Int 133: 390-406.

Arger J, Milcheli J, Westaway R (1996). Neogene and Quaternary Volcanism of Eastern Turkey: Potassium-Argon Dating and Its Tectonic Implications. Open-file Science Reports. 1996/1. Newcastle upon Tyne, UK: Technoscience.

Arpat E, Şaroğlu F (1972). The East Anatolian Fault System: thoughts on its development. Bulletin of the Mineral Research and Exploration (MTA) 78: 33-39.

Arpat E, Şaroğlu F (1975). Recent tectonic activities in Turkey. Bulletin of the Geological Society of Turkey 18: 91-101 (in Turkish with English abstract).

Azañón JM, Pérez-Peña JV, Giaconia F, Booth-Rea1 G, Martínez-Martínez JM, Rodríguez-Peces MJ (2012). Active tectonics in the central and eastern Betic Cordillera through morphotectonic analysis: the case of Sierra Nevada and Sierra Alhamilla. J Iber Geol 38: 225-238.

Azor A, Keller EA, Yeats RS (2002). Geomorphic indicators of active fold growth: South Mountain-Oak Ridge anticline, Ventura basin, southern California. Geol Soc Am Bull 114: 745-753.

Barka AA, Kadinsky-Cade K (1988). Strike-slip fault geometry in Turkey and its influence on earthquake activity. Tectonics 7: 663-684.

Bull WB (1977). The alluvial fan environment. Prog Phys Geog 1: 22-270.

Bull WB, McFadden LD (1977). Tectonic geomorphology north and south of the Garlock fault, California. In: Doehering O, editor. Geomorphology in Arid Regions. The 8th Annual Geomorphology Symposium Proceedings. Binghamton, NY, USA: State University of New York, pp. 115-138.

Bulut F, Bohnhoff M, Eken T, Janssen C, Kılıç T, Dresen G (2012). The East Anatolian Fault Zone: Seismotectonic setting and spatiotemporal characteristics of seismicity based on precise earthquake locations. J Geophys Res 117: 1-16.

Castelltort S, Goren L, Willett S, Champagnac J, Herman F, Braun J (2012). River drainage patterns in the New Zealand Alps primarily controlled by plate tectonic strain. Nat Geosci 16: 1-5.

Çetin H, Güneyli H, Mayer L (2003). Paleosismology of the Palu-Lake Hazar segment of the East Anatolian Fault Zone, Turkey. Tectonophysics 374: 163-197.

Dewey JF, Hempton MR, Kidd WSF, Şaroglu F, Şengör AMC (1986). Shortening of continental lithosphere: the neotectonics of Eastern Anatolia - a young collision zone. In: Coward MP, Ries AC, editors. Collision Tectonics. London, UK: Geological Society of London Special Publications, pp. 3-36.

Duman TY, Emre Ö (2013). The East Anatolian Fault: geometry segmentation and jog characteristics. Geol Soc London Spec Publ 372: 495-529.

El Hamdouni R, Irigaray C, Fernandez T, Chacón J, Keller EA (2008). Assessment of relative active tectonics, southwest border of Sierra Nevada (southern Spain). Geomorphology 96: 150-173.

Emre Ö, Duman TY, Özalp S, Elmaci H, Olgun Ş, Şaroğlu F (2013). Active Fault Map of Turkey with an Explanatory Text. Ankara, Turkey: General Directorate of Mineral Research and Exploration (MTA).

Farr TG, Rosen PA, Caro E, Crippen R, Duren R, Hensley S, Kobrick M, Paller M, Rodrigue ZE, Roth L et al. (2007). The shuttle radar topography mission. Rev Geophys 45: 1-33.

Hack JT (1973). Stream profile analysis and stream-gradient index. J Res US Geol Surv 1: 421-429.

Hempton MR (1985). Structure and deformation history of Bitlis suture near Lake Hazar, southeastern Turkey. Bull Geo Soc Am 96: 233-243.

Hempton MR (1987). Constraints on Arabian plate motion and extensional history of the Red Sea. Tectonics 6: 687-705.

Hempton MR, Dewey JF, Şaroğlu F (1981). The East Anatolian transform fault: along strike variations in geometry and behavior. EOS T AM Geophys UN 62: 393.

Herece E (2008). Atlas of the East Anatolian Fault. Ankara, Turkey: General Directorate of Mineral Research and Exploration (MTA), Special Publication Series.

Herece E, Akay E (1992). Karlıova-Çelikhan arasında Doğu Anadolu Fayı, Turkiye. Petrol Kongresi Bildirileri. In: 9th Petroleum Congress of Turkey Proceedings, 17–21 February 1992, Ankara, Turkey, pp. 361-372 (in Turkish).

Hubert-Ferrari A, King G, Vander Woerd J, Villa I, Altunel E, Armijo R (2009). Long-term evolution of the North Anatolian Fault: new constrains from its eastern termination. In: Van Hinsbergen DJJ, Edwards MA, Govers R, editors. Collision and Collapse at the Africa-Arabia-Eurasia Subduction Zone. London, UK: Geological Society of London Special Publication, pp. 133-154.

Jackson J, McKenzie DP (1984). Active tectonics of the Alpine-Himalayan belt between western Turkey and Pakistan. Geophys J Roy Astr S 77: 185-264.

Karabacak V, Önder Y, Altunel E, Yalçıner CC, Akyüz HS, Kıyak NG (2011). Doğu Anadolu Fay Zonunun güney batı uzanımının paleosismolojisi ve ilk kayma hızı. In: Proceedings of Aktif Tektonik Araştırma Grubu Onbeşinci Çalıştayı, 19–22 October 2011, Adana, Turkey (in Turkish).

Kaymakcı N, İnceöz M Ertepınar P (2006). 3D-Architecture and Neogene evolution of the Malatya Basin: inferences for the kinematics of the Malatya and Ovacık Fault zones. Turkish J Earth Sci 15:123-154.

Keller EA, DeVecchio DE (2013). Tectonic geomorphology of active folding and development of transverse drainage. In: Shroder J, Owen LA, editors. Treatise on Geomorphology. 5th ed. San Diego, CA, USA: Academic Press, pp. 129-147.

Keller EA, Pinter N, editors (2002). Active Tectonics: Earthquakes, Uplift and Landscapes. 2nd ed. Upper Saddle River, NJ, USA: Prentice Hall.

Khalifa A, Çakır Z, Owen LA, Kaya Ş (2017). Evaluation of the relative tectonic activity of the Adıyaman Fault in Eastern Turkey. Conference abstract. In: International Symposium on GIS Applications in Geography and Geosciences, 18–21 October 2017, Çanakkale, Turkey, p. 293.

Kiratzi A (1993). A study on the active crustal deformation of the North and East Anatolian Fault Zones. Tectonophysics 225: 191-203.

Koçyiğit A, Beyhan A (1998). A new intracontinental transcurrent structure: the Central Anatolian Fault Zone, Turkey. Tectonophysics 284: 317-336.

Langbein WB (1947). Topographic Characteristics of Drainage Basins. Water Supply Paper 968-C. Washington, DC, USA: US Geological Survey.

Mahmoud Y, Masson F, Meghraoui M, Cakir Z, Alchalbi A, Yavasoglu H, Yönlü Ö, Daoud M, Ergintav S, Inan S (2013). Kinematic study at the junction of the East Anatolian fault and the Dead Sea fault from GPS measurements. J Geodyn 67: 30-39.

Mayer L, editor (1990). Introduction to Quantitative Geomorphology: An Exercise Manual. Englewood Cliffs, NJ, USA: Prentice Hall.

McKenzie DP (1972). Active tectonics of the Mediterranean region. Geophys J Int 30: 109-185.

McKenzie DP (1976). The East Anatolian fault: a major structure in eastern Turkey. Earth Planet Sc Lett 29: 189-193.

McKenzie DP (1978). Active tectonics of the Alpine- Himalayan belt: The Aegean Sea and surrounding regions (tectonic of Aegean region). Geophys J Roy Astr S 55: 217-254.

Meghraoui M, Bertrand S, Karabacak V, Ferry M, Çakir Z, Altunel E (2006). Surface ruptures along the Maras segment of the East Anatolian Fault (SE Turkey) and kinematic modelling from Tectonic and GPS data. Geophysical Research Abstracts 8: 10006.

Melosh B, Keller EA (2013). Effects of active folding and reverse faulting on stream channel evolution, Santa Barbara Fold Belt, California. Geomorphology 186: 119-135.

Michael K, Frank L (2013). Geomorphology of the Tsetseg Nuur basin, Mongolian Altai-lake development, fluvial sedimentation and aeolian transport in a semi-arid environment. J Maps 9: 361-366.

Moreno DG, Hubert-Ferrari A, Moernaut J, Fraser JG, Boes X, Van Daele M, Avsar U, Çağatay N, De Batist M (2010). Structure and recent evolution of the Hazar Basin: a strike-slip basin on the East Anatolian Fault, Eastern Turkey. Basin Res 23: 191-207.

Muehlberger WR, Gordon MB (1987). Observations on the complexity of the East Anatolian Fault, Turkey. J Struct Geol 9: 899-903.

Owen LA, Cunningham WD, Brian FW, Badamgarov J, Dorjnamjaa D (1999). The landscape evolution of Nemegt Uul: a late Cenozoic transpressional uplift in the Gobi Altai, southern Mongolia. Geol Soc London Spec Publ 162: 201-218.

Özkaymak C, Sözbilir H (2012). Tectonic geomorphology of the Spreader High Ranges, Western Anatolia. Geomorphology. 173-174: 128-140.

Pike RJ, Wilson SE (1971). Elevation-relief ratio, hypsometric integral and geomorphic area-altitude analysis. Geol Soc Am Bull 82: 1079-1084.

Reilinger R, McClusky S, Vernant P, Lawrence S, Ergintav S, Cakmak R, Ozener H, Kadirov F, Guliev I, Stepanyan R et al. (2006). GPS constraints on continental deformation in the Africa-Arabia–Eurasia continental collision zone and implications for dynamics of plate interactions. J Geophys Res 111: 1-26.

Rockwell TK, Keller EA, Johnson DL (1984). Tectonic geomorphology of alluvial fans and mountain fronts near Ventura, California. In: Morisawa M, Hack JT, editors. Tectonic Geomorphology. The 15th Annual Geomorphology Symposium Proceedings. Boston, MA, USA: Allen and Unwin, pp. 183-207.

Şaroğlu F, Emre Ö, Kuşçu I (1992a). Active fault map of Turkey. Ankara, Turkey: General Directorate of Mineral and Research Exploration of Turkey Publication (MTA).

Şaroğlu F, Emre Ö, Kuşçu I (1992b). The East Anatolian fault zone of Turkey. Annales Tectonicae 6: 99-125.

Selby MJ (1980). A rock strength classification for geomorphic purposes: with tests from Antarctica and New Zealand. Z Geomorphol 24: 31-51.

Selçuk AS (2016). Evaluation of the relative tectonic activity in the eastern Lake Van basin, East Turkey. Geomorphology 270: 9-21.

Şengör AMC (1979). The North Anatolian Transform Fault: its age, offset and tectonic significance. Geol Soc London Spec Publ 136: 269-282.

Şengör AMC, Görür N, Şaroğlu F (1985). Strike slip faulting and related basin formation in zones of tectonic escape: Turkey as a case study. In: Biddle KT, Christie-Blick N, editors. Strike-Slip Deformation, Basin Formation and Sedimentation. Tulsa, OK, USA: Society of Economic Paleontologists and Mineralogists, pp. 227-264.

Şengör AMC, Grall C, Imren C, Le Pichon X, Görür N, Henery P, Karabulut H, Siyako S (2014). The geometry of the North Anatolian transform fault in the Sea of Marmara and its temporal evolution: implications for the development of intracontinental transform faults. Can J Earth Sci 51: 222-242.

Silva PG, Goy JL, Zazo C, Bardaji T (2003). Fault-generated mountain fronts in southeast Spain: geomorphologic assessment of tectonic and seismic activity. Geomorphology 50: 203-225.

Strahler AN (1952). Hypsometric (area-altitude curve) analysis of erosional topography. Geol Soc Am Bull 63: 1117-1141.

Tari U, Tüysüz O (2015). The effects of the North Anatolian Fault on the geomorphology in the Eastern Marmara Region, Northwestern Turkey. Geodin Acta 28: 139-159.

Taymaz T, Eyidoğan H, Jackson J (1991). Source parameters of large earthquakes in the East Anatolian Fault Zone (Turkey). Geophys J Int 106: 537-50.

Tepe Ç, Sözbilir H (2017). Tectonic geomorphology of the Kemalpaşa Basin and surrounding horsts, southwestern part of the Gediz Graben, Western Anatolia. Geodin Acta 29: 70-90.

Topal S, Keller E, Bufe A, Koçyiğit A (2016). Tectonic geomorphology of a large normal fault: Akşehir fault, SW Turkey. Geomorphology 259: 55-69.

Ul-Hadi S, Shuhab DK, Owen LA, Khan AS (2013). Geomorphic response to an active transpressive regime: a case study along the Chaman strike-slip fault, western Pakistan. Earth Surf Proc Land 38: 250-264.

Westaway R (1994). Present-day kinematics of the Middle East and eastern Mediterranean. J Geophys Res 99: 12071-12090.

Westaway R, Arger J (1996). The Gölbaşı basin, southeastern Turkey: a complex discontinuity in a major strike-slip fault zone. Geol Soc London Spec Publ 153: 729-743.

Westaway R, Arger J (2001). Kinematics of the Malatya-Ovacık Fault Zone. Geodin Acta 14: 103-131.

Westaway R, Demir T, Seyrek A, Beck A (2006). Kinematics of active left-lateral faulting in SE Turkey from offset Pleistocene river gorges: improved constraint on the rate and history of relative motion between the Turkish and Arabian plates. Geol Soc London Spec Publ 163: 149-164.

Yalçın MN (1979). Dogu Anadolu yarılımının Türkoğlu-Karaağaç (K. Maraş) arasındaki kesiminin özellikleri ve bölgedeki yerleşim alanları. In: Türkiye Jeologi Kurumu Altınlı Simpozyumu, Özel Sayı, pp. 49-55 (in Turkish).

Yıldırım C (2014). Relative tectonic activity assessment of the Tuz Gölü Fault Zone; Central Anatolia, Turkey. Tectonophysics 630: 183-192.

Yönlü Ö, Altunel E, Karabacak V (2017). Geological and geomorphological evidence for the southwestern extension of the East Anatolian Fault Zone, Turkey. Earth Planet Sc Lett 469: 1-14.

Yönlü Ö, Altunel E, Karabacak V, Serdar Akyüz H (2013). Evolution of the Gölbaşı basin and its implications for the long-term offset on the East Anatolian Fault Zone, Turkey. J Geodyn 65: 272-281.

Yönlü Ö, Karabacak V, Altunel E, Akyüz HS (2012). Paleoseismological slip rate on the East Anatolian fault zone around Türkoğlu. Conference abstract. In: International Earth Science Colloquium on the Aegean Region, 1–5 October 2012, İzmir, Turkey, p. 104.

Yürür MT, Chorowicz J (1998). Recent volcanism, tectonics and plate kinematics near the junction of the African, Arabian and Anatolian plates in the Eastern Mediterranean. J Volcanol Geotherm Res 85: 1-15.